ChemPhotoChem

Research Article
doi.org/10.1002/cptc.202400117

Chemistry Europe
European Chemical Societies Publishing

www.chemphotochem.org

Optical Emission Spectra of Molecular Excitonic Polariton Computed at the First-Principles Level QED-TDDFT

Shanhao Deng,[a] Junjie Yang,[b] Yihan Shao,[c] Qi Ou,*[d] and Zhigang Shuai*[a, e]

In microcavity, strong coupling between light and molecules leads to the formation of hybrid excitations, i.e., the polaritons, or exciton-polaritons. Such coupling may alter the energy landscape of the system and the optical properties of the material, making it an effective approach for controlling the light emission from molecular materials. However, due to the complexity of vibrational modes, spectroscopic calculations for organic exciton-polaritons remain to be challenging. In this work, based on the linear-response quantum-electrodynamical time-dependent density functional theory (QED-TDDFT), we employ the thermal vibrational correlation function (TVCF) formalism to calculate the molecular optical spectrum of the lower polaritons (LP) at first-principles level for three molecules, i.e., anthracene, distyrylbenzenes (DSB), and rubrene. The polaron decoupling effect is confirmed from our first-principles computations. The theoretical emission spectra of LP provide new insights for aiding molecular and device design in microcavities that are otherwise hindered due to the lack of vibrational information.

1. Introduction

Inside an optical cavity, molecules may strongly interact with space-quantized photon, namely the cavity modes, to generate a new hybrid excited state, known as exciton-polariton (or polariton).[1–6] The formation of the polariton may remarkably alter the energy landscape of the system and the physical and chemical properties of the material, such as chemical reactivity[7–10] and excited-state dynamics.[11–16] The extent of such changes depends on the strength of the light-matter coupling.[17] Importantly, polaritons have the ability to freely interconvert with unbound photons outside the cavity,[5] providing a simple and effective approach for controlling the light emission of molecular materials. This concept holds great potential for applications in next-generation optoelectronic devices, such as sensors,[18–20] optoelectronic integrated circuits,[21] light-emitting diodes,[22–24] and even room-temperature exciton-polariton lasers.[25–28]

It is challenging to calculate the exciton-polariton optical spectra at the first-principles level for complex molecules, which usually requires the introduction of significant approximations in the calculations.[29] Although some optical spectra have been calculated using model Hamiltonians,[30–35] limited information is provided compared to the rich vibrational characteristics of organic molecules. Spano and coworkers have made predictions based on the resonant Holstein-Tavis-Cummings (HTC) model.[31,32,36,37] For both single molecules and aggregates, as the cavity coupling strength increases, the relative intensity of the system's emission, exhibits an increase at the 0–0 vibrational peak and a decrease at the 0–1 vibrational peak. This trend is accompanied by a decrease in the reorganization energy, indicating an effective decoupling between the electronic and vibrational degrees of freedom, commonly referred to as polaron decoupling.[32] It is intriguing to demonstrate such effect at the first-principles level by incorporating quantum electrodynamics into quantum chemistry calculations.

In recent years, significant progress has been made in the development of first-principles methods for polaritons, such as quantum-electrodynamical time-dependent density functional theory (QED-TDDFT),[38–45] quantum electrodynamics coupled-cluster (QED-CC).[46,47] These methods enable us to accurately describe the molecular electronic structure of polaritons in a way comparable to conventional organic molecules. Furthermore, the work by Yang and coworkers on the analytical energy gradients of QED-TDDFT has facilitated the direct vibrational analysis of polaritons formed within optical cavities containing realistic molecules.[45] In combination with the thermal vibrational correlation function (TVCF) method, which has been widely used for the computation of organic molecule spectra and rates of photophysical processes,[48–51] in this work, we calculate the optical spectra for molecular polaritons with vibronic resolutions at the first-principles level, for anthracene,

[a] S. Deng, Prof. Z. Shuai
Department of Chemistry, MOE Key Laboratory of Organic OptoElectronics and Molecular Engineering, Tsinghua University, 100084 Beijing, China

[b] J. Yang
Division of Chemistry and Chemical Engineering, California Institute of Technology, Pasadena, California 91125, USA

[c] Y. Shao
Department of Chemistry and Biochemistry, University of Oklahoma, Norman, Oklahoma 73019, USA

[d] Q. Ou
SINOPEC Research Institute of Petroleum Processing Co., Ltd, Beijing, 100083, China
E-mail: ouqi.ripp@sinopec.com

[e] Prof. Z. Shuai
School of Science and Engineering, The Chinese University of Hong Kong, Shenzhen, 518172 Guangdong, ChinSchool of Science and Engineering, The Chinese University of Hong Kong, Shenzhen, 518172 Guangdong, China
E-mail: shuaizhigang@cuhk.edu.cna
shuaizhigang@cuhk.edu.cn

Supporting information for this article is available on the WWW under https://doi.org/10.1002/cptc.202400117

DSB, and rubrene, see Figure 1(a). We aim to calculate the optical emission spectra of LP for these prototypical light-emitting molecules in order to deepen the understanding of strong light-matter coupling at the level of molecular spectrum.

2. Theoretical Formalism and Computational Methods

In this study, we investigate a straightforward system consisting of a single molecule coupled to a single-mode Fabry-Perot cavity. The electronic structure calculations are based on the Jaynes-Cummings model within the Tamm-Dancoff approximation (TDA), namely the TDA-JC model, which neglects the dipole self-energy (DSE) and counter-rotating terms (CRTs) and reads[44]

$$\begin{bmatrix} \boldsymbol{A} & \hbar\mathbf{g}^{\dagger} \\ \hbar\mathbf{g} & \hbar\omega_C \end{bmatrix} \begin{bmatrix} \boldsymbol{X} \\ M \end{bmatrix} = E_{TDA-JC} \begin{bmatrix} 1 & 0 \\ 0 & 1 \end{bmatrix} \begin{bmatrix} \boldsymbol{X} \\ M \end{bmatrix} \tag{1}$$

where the electronic-electronic block $\boldsymbol{A}$ corresponds to the super-operator used in TDDFT/TDA, and ω_C denotes the frequency of the cavity mode. The electronic-photon block is represented as:

$$\hbar g_{bj} = \sqrt{\frac{\hbar\omega_C}{2}}\boldsymbol{\lambda} \cdot \boldsymbol{\mu}_{bj} \tag{2}$$

$\boldsymbol{\mu}_{bj} = \langle b|\hat{\boldsymbol{r}}|j\rangle$, represents the transition dipole between the unoccupied Kohn-Sham orbital b and the occupied orbital j. $\boldsymbol{\lambda}$ is the fundamental coupling strength,[41,44] of which the absolute value is proportional to the amplitude of the vacuum electric field at the position of the molecule and parallel to the polarization direction of the cavity mode. In the calculations, $\boldsymbol{\lambda}$ is treated as an adjustable parameter. The I^{th} solution of the equation: E^{I}_{TDA-JC} represents the excitation energy of the I^{th} polaritonic state $|\phi_I\rangle$ in the TDA-JC model. $\boldsymbol{X}^{I}$ and M^{I} are the corresponding TDA-JC amplitudes, satisfying the normalization condition:

$$\sum_{a,i} X^{I}_{ai} X^{J}_{ai} + M^{I} M^{J} = \delta_{IJ} \tag{3}$$

where the first term represents the contribution of the electronic excited state, while the second term represents the photon contribution (Hopfield coefficient).We quantify the light-matter coupling strength associated with the state $|\phi_I\rangle$ using the light-matter interaction energy, which is expressed as follows:

$$E^{I}_{ele-ph} = 2\hbar M^{I}\mathbf{g} \cdot \boldsymbol{X}^{I} = \sqrt{2\hbar\omega_C} M^{I}\boldsymbol{\lambda} \cdot \boldsymbol{\mu}^{I} \tag{4}$$

where $\boldsymbol{\mu}^{I} = \sum_{b,j} X^{I}_{bj}\boldsymbol{\mu}_{bj}$, is the transition dipole moment of $|\phi_I\rangle$.

The spectral function of the cavity leakage can be represented as the Fourier transform of the cavity field autocorrelation function, given by[32]

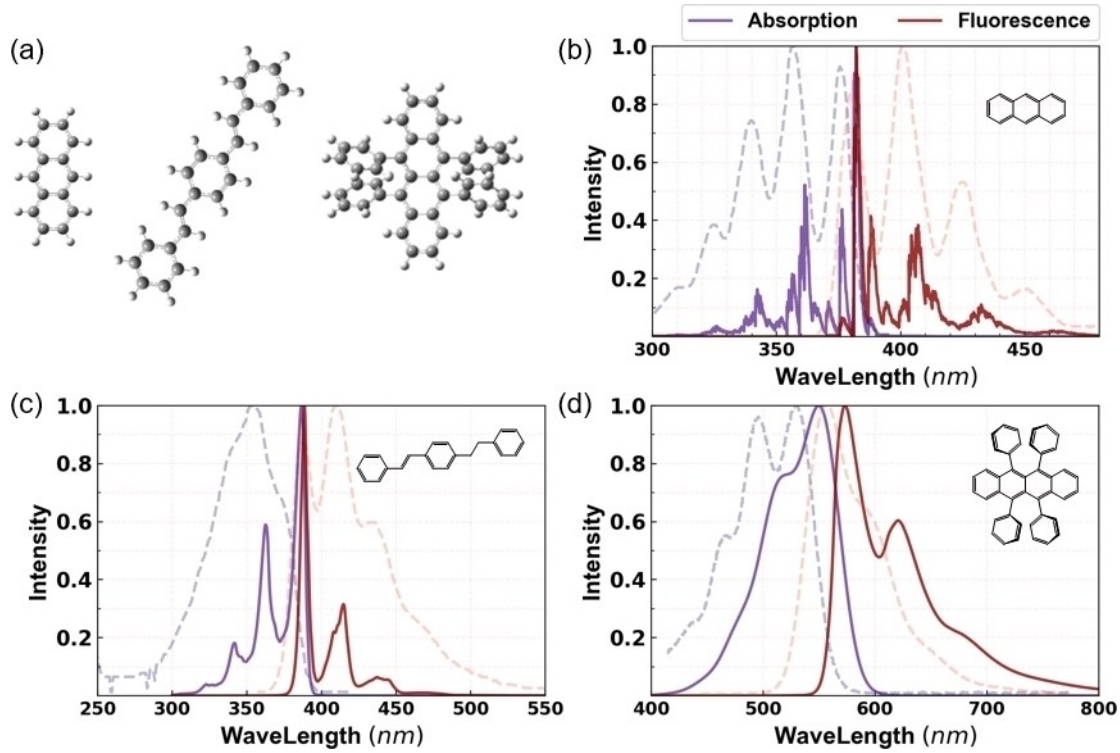

Figure 1. (a) Molecular structures of three investigated systems in this work. Theoretically predicted absorption (purple) and emission (red) spectra of (b) anthracene, (c) DSB, (d) rubrene. Experimental spectra are represented by dashed lines in the background, adapted from refs.[61–63]

$$S(\omega) \propto Re\int_0^{\infty} d\tau\langle\hat{a}^{\dagger}(t+\tau)\hat{a}(t)\rangle e^{-i\omega\tau} = \pi\sum_{i,f} P_i|\langle\Psi_f|\hat{a}|\Psi_i\rangle|^2\delta(\omega_{i,f}-\omega) \quad (5)$$

The above expression is derived because "for a classical (coherent state) input field that is uncorrelated with the intracavity field operator $\hat{a}(t)$, i.e., $\langle\hat{F}_1(t)\hat{a}(t')\rangle \rightarrow 0$, the external field spectrum is directly proportional to the spectrum of the intracavity field fluctuations."[32] The input-output relations for the cavity can be found in S1 of Supporting Information and the derivation is based on ref.[53] Where $|\Psi_i\rangle$ and $|\Psi_f\rangle$ represent the initial and final states of the transition, E_i and E_f are the respective energies, $\omega_{i,f} = (E_i - E_f)/\hbar$, P_i is the Boltzmann distribution function of the initial state, and $\hat{a}$ and $\hat{a}^{\dagger}$ represent the annihilation and creation operators of the cavity mode photons. To obtain the emission spectrum of LP that includes vibrational information, the initial and final states in Eq. (5) are set to be the different vibrational energy levels of the LP state $|\Phi_{LP}\rangle$ and the ground state $|\Phi_G\rangle$. Under the adiabatic approximation, the system's state can be written as a product of the electronic-photon part $|\Phi\rangle$ and the vibrational part $|\Theta\rangle$. Therefore, the spectrum can be expressed as:

$$S(\omega) \propto \pi|\langle\Phi_G|\hat{a}|\Phi_{LP}\rangle|^2 P_{LP\nu_{LP}}(T)\delta(\omega_{LP\nu_{LP},G\nu_G}-\omega)\left|\langle\Theta_{G\nu_G}|\Theta_{LP\nu_{LP}}\rangle\right|^2 \quad (6)$$

where $|\langle\Phi_G|\hat{a}|\Phi_{LP}\rangle|^2 = \left|\sum_{a,i}\langle\Psi_G|\hat{a}|\Psi_a^i\rangle X_{ai} + \langle 0|\hat{a}|1\rangle M_{LP}\right|^2 = \left(M^{LP}\right)^2$ is the photon contribution of LP, where $\left|\Psi_a^i\right\rangle$ represents a singly excited state with an electron excited from orbital a to orbital i. $|\Theta_{i,\nu_i}\rangle$ represents the system in the ν_i-th vibrational state, and $P_{LP\nu_{LP}}(T)$ follows the Boltzmann distribution at temperature T. Through expressing the Dirac-delta function by a Fourier time series and inserting complete basis, Eq. (6) can be expressed in the form of TVCF as follows:

$$\sum_{\nu_{LP},\nu_G} P_{LP\nu_{LP}}(T)\delta(\omega_{LP\nu_{LP},G\nu_G}-\omega)\left|\langle\Theta_{G\nu_G}|\Theta_{LP\nu_{LP}}\rangle\right|^2 = \frac{1}{2\pi}\int_{-\infty}^{+\infty} dt e^{-i\left(\omega-\omega_{LP\nu_{LP},G\nu_G}\right)t}\left[Z_{LP}^{-1}\rho_{LP,G}(t,T)\right]\# \quad (7)$$

where Z_{LP} is the partition function of the LP state, and $\rho_{LP,G}(t,T) = Tr\left[e^{-iH_f t}e^{-iH_i t_i}\right]$, represents the correlation function corresponding to the LP emission process.[49,52] Where $t_i = -\frac{i}{kT} - t$, k is the Boltzmann constant, and H_f and H_i represent the final and initial state vibrational Hamiltonians, respectively.

In order to obtain vibrational information of the molecule, we need to diagonalize the matrix of molecular force constants weighted by atomic masses:

$$\boldsymbol{\omega}_{\nu} = \boldsymbol{L}_{norm}^{T}\boldsymbol{M}^{-\frac{1}{2}}\boldsymbol{F}\boldsymbol{M}^{-\frac{1}{2}}\boldsymbol{L}_{norm} \quad (8)$$

Where $F_{xy} = \frac{\partial^2 E}{\partial R_x \partial R_y}\Big|_{R_0}$, $\boldsymbol{M} = diag(m_1, m_1, m_1, m_2 \ldots m_N)$, $\boldsymbol{R}$ represents the 3 N coordinates of N atoms, $\boldsymbol{R}_0$ denotes the equilibrium position, m is the atomic mass, $\boldsymbol{F}$ and $\boldsymbol{M}$ are both 3 N×3 N matrices. The canonical vibrational frequencies (3 N-6 for nonlinear molecules) $\boldsymbol{\omega}_{\nu}$ and the corresponding canonical coordinates are obtained:

$$\boldsymbol{Q} = \boldsymbol{L}_{norm}^{T}\boldsymbol{M}^{\frac{1}{2}}(\boldsymbol{R} - \boldsymbol{R}_0) \quad (9)$$

For absorption and emission processes, the relationship between initial and final state canonical coordinates is satisfied:

$$\boldsymbol{Q}_f = \boldsymbol{J}_{f\leftarrow i}\boldsymbol{Q}_i + \boldsymbol{K}_{f\leftarrow i} \quad (10)$$

The Duschinsky rotation matrix $\boldsymbol{J}_{f\leftarrow i} = \boldsymbol{L}_{norm,f}^{T}\boldsymbol{L}_{norm,i}$, and the mode displacement $\boldsymbol{K}_{f\leftarrow i} = \boldsymbol{L}_{norm,f}^{T}\boldsymbol{M}^{1/2}(\boldsymbol{R}_{i0} - \boldsymbol{R}_{f0})$. Here, the equilibrium positions of the initial and final states are translated and rotated to satisfy the Eckart conditions.[54] The Huang-Rhys factor for the k^{th} mode is represented as $s_{f\leftarrow i,k} = \frac{1}{2}\omega_{f,k}K_{f\leftarrow i,k}$, and the corresponding mode reorganization energy is $\Delta E_{Rf\leftarrow i,k} = \omega_{f,k}s_{f\leftarrow i,k}$. We quantify the strength of the electronic-vibrational coupling in the excited state using the total reorganization energy $\Delta E_{Rf\leftarrow i,} = \sum_k \omega_{f,k}s_{f\leftarrow i,k}$.

The TDA-JC model used in this work for energy and analytical gradient calculations were implemented by Yang *et al.* in a development version of the PySCF software package.[44,45] The polarization parameter $\boldsymbol{\lambda}$ is set to be parallel to the transition dipole moment of the S_1 excited state to prevent significant molecular re-orientation during the structure optimization process. The TDA-JC method reduces to TDA when there is no electromagnetic mode, and can be directly computed using the original PySCF.[55–57] The functional and basis set are consistently set to B3LYP/6-31G* level. After completing the structure optimization, the second-order energy derivative of the LP state is obtained using numerical differentiation with a step size of 0.001 atomic units, which is then fed to the molecular property prediction program MOMAP to obtain the LP emission spectra via the analytical calculation of TVCF.[49,58,59] In the visualization of ground state vibrational modes, the ground state Hessian matrix was calculated by Gaussian 16[60] with the B3LYP functional and the basis set 6–31G* to obtain a Hermitian Hessian matrix.

3. Results and Discussion

The structure of the investigated molecules is presented in Figure 1(a). We first perform the electronic structure calculations and conduct structural optimization without incorporating the electromagnetic mode. The calculated properties are summarized in Table 1. Additional excitation energies and transition dipole moments for more excited states are provided in Tables S1–S3.

Under the absence of the cavity electromagnetic mode, we compute the absorption and emission spectra of the three molecules at 300 K, are displayed in Figure 1 (b–d). It can be

Table 1. Calculated vertical excitation energies of S_1 under optimized S_0 and S_1 geometries, i.e., absorption energy (E_{abs}) and emission energy (Eemi), adiabatic excitation energy of S_1 (Ead), transition dipole of S_1 at S_0 geometry (μ), $S_1 \rightarrow S_0$ reorganization energy obtained from vibrational analysis (ΔE_R), and from the four-point method ($\Delta E'_R$) for the three molecules.

Molecule	Eabs (eV)	Eemi (eV)	Ead (eV)	μ (a.u.)	ΔE_R (cm^{-1})	$\Delta E'_R$ (cm^{-1})
anthracene	3.506	3.184	3.341	1.021	1316	1262
DSB	3.380	3.114	3.236	5.453	1023	984
rubrene	2.412	2.086	2.243	2.070	1191*	1267

[*] This result was computed using internal coordinates.

Table 2. Photon energies ($\hbar\omega_c$) and Detuning levels of the four cavity cases considered in this work.

Case	Molecule	$\hbar\omega_c$ (eV)	Detuning (eV)
1	anthracene	3.506	0.165
2	anthracene	3.184	−0.156
3	DSB	3.380	0.144
4	rubrene	2.412	0.169

observed that the calculated spectra exhibit similar relative vibrational peak positions as compared to the experimental spectra, indicating that the computational results can effectively capture the vibrational structures of the S_0 and S_1 state of these molecules. Figure 2 illustrates the distribution of $S_1 \rightarrow S_0$ reorganization energies. For anthracene and DSB, their reorganization energies concentrate on high-frequency modes, primarily corresponding to the stretching of C–C bonds and the bending of C–H bonds. In contrast, rubrene mode 1 exhibits a significant reorganization energy distribution and a larger Huang-Rhys factor, corresponding to the rotation of phenyl groups. Therefore, despite the three molecules having similar total reorganization energies, the S_1 and S_0 structures of anthracene and DSB almost overlap, while those of rubrene exhibit significant differences, as shown in Figure S1. Additionally, the rubrene spectrum also features a more significant 0–1 peak, as shown in Figure 1. In the vibrational analysis and spectral calculations of rubrene, we employed internal coordinates, which are considered more effective for flexible molecules.[64–66] In contrast, using Cartesian coordinates for the vibrational analysis resulted in a significantly unrealistic reorganization energy (2507 cm^{-1}).

Next, we incorporate the electromagnetic modes onto three molecules. For simplicity, we only consider four cases as shown in Table 2: resonances between the cavity mode frequency $\hbar\omega_C$ and the absorption energies of three molecules in **cases 1**, **3**, and **4**, as well as resonance with the emission energy of anthracene in **case 2**. Due to the variation of the S_1 excitation energy with the molecular structure during the LP structure optimization process, we define the detuning as the difference between the cavity mode energy and the adiabatic excitation energy of the molecule's S_1 state, as shown in Scheme 1. The fundamental coupling strength is chosen to be parallel to the transition dipole moment of the first excited state. We perform geometry optimization of the LP state in the system with respect to varied values of λ and calculate the excitation energies and photon contributions of the first two excited states, i.e., LP and upper polariton (UP), as shown in panel a of Figures 3–6. For anthracene, additional optimization results of LP under various cavity mode energies are displayed in Figure S3. Panel b of Figures 3–6 demonstrates the corresponding relationship between the light-matter interaction energy of LP and λ, where for all **cases 1**–**4**, the interaction energy exhibits a monotonical increase with λ.

In the following discussion, we first consider **cases 1** and **2**. We first analyze the energy levels of the LP and UP. As λ approaches 0, the energy difference between UP and LP not being entirely zero due to the detuning. The potential energy surfaces for both negative and positive detuning (**cases 1** and **cases 2**) as well as the resonant case (where the photon energy equals the adiabatic excitation energy) are shown in Figures S4–S6. As λ increases, the energy of LP decreases while the energy of UP increases, resulting in an expected increase in the energy splitting between LP and UP. At lower values of λ, the energy change is not significant, and for the case of negative detuning (**cases 2**), the decrease in LP energy occurs earlier as compared to the positive detuning (**cases 1**). In both **cases 1** and **cases 2**, the slope of the LP energy relative to λ is similar and corresponds to an increasing light-matter interaction energy. However, for the case where the cavity mode energy is closer to the adiabatic excitation energy, i.e., smaller detuning, the coupling strength increases more prominently with respect to λ, as shown in Figure S7 (when $\hbar\omega_C$ =3.265 eV, corresponding to 0.120 a.u.). Consequently, the slope of LP energy decrease during this phase is larger, as shown in Figure S3(b).

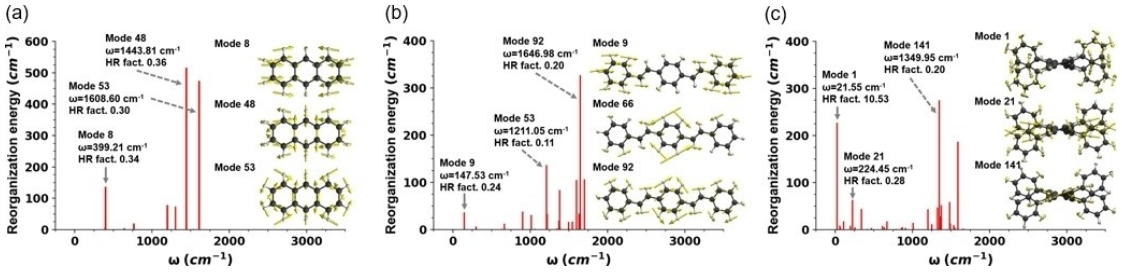

Figure 2. Decomposition of the reorganization energies of (a) anthracene, (b) DSB and (c) rubrene The three vibrational modes of S_0 with the largest three Huang-Rhys (HR) factors are visualized in the insets.

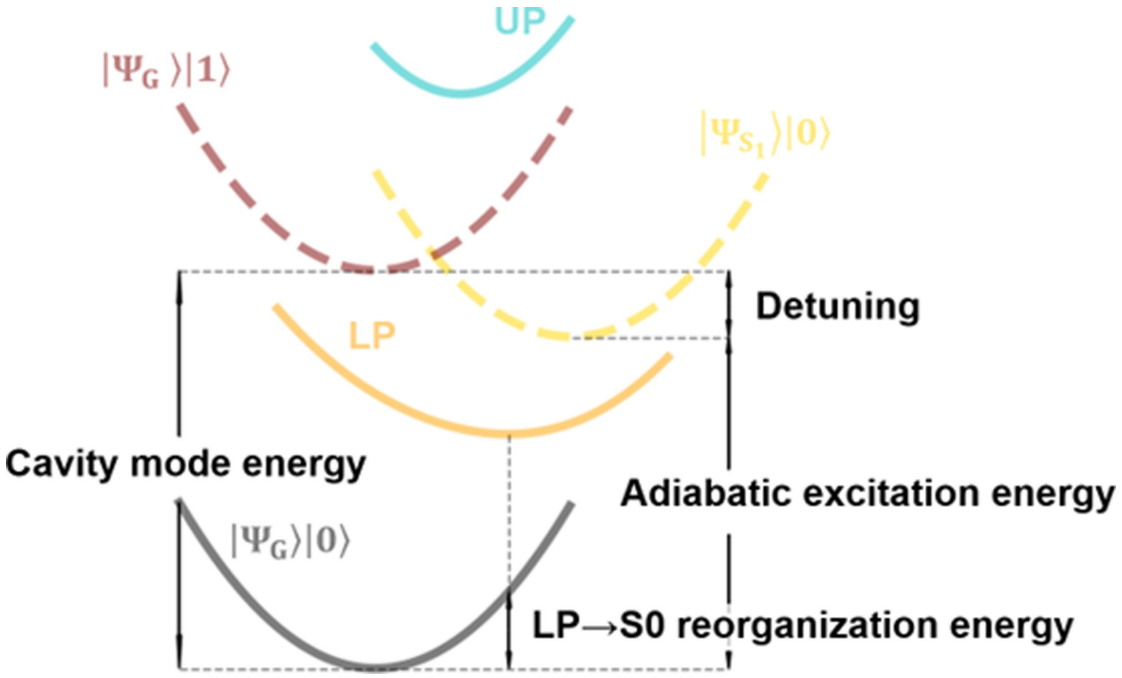

Scheme 1. Schematic representation of the potential energy surfaces under strong coupling between the molecule and the cavity mode.

Due to the influence of higher excited states, the energy increase of UP is suppressed, resulting in an asymmetric splitting.[44] For the case of a large positive detuning with a cavity mode energy of 3.673 eV (corresponding to 0.135 a.u.), as shown in Figure S3(d), the UP composition gradually

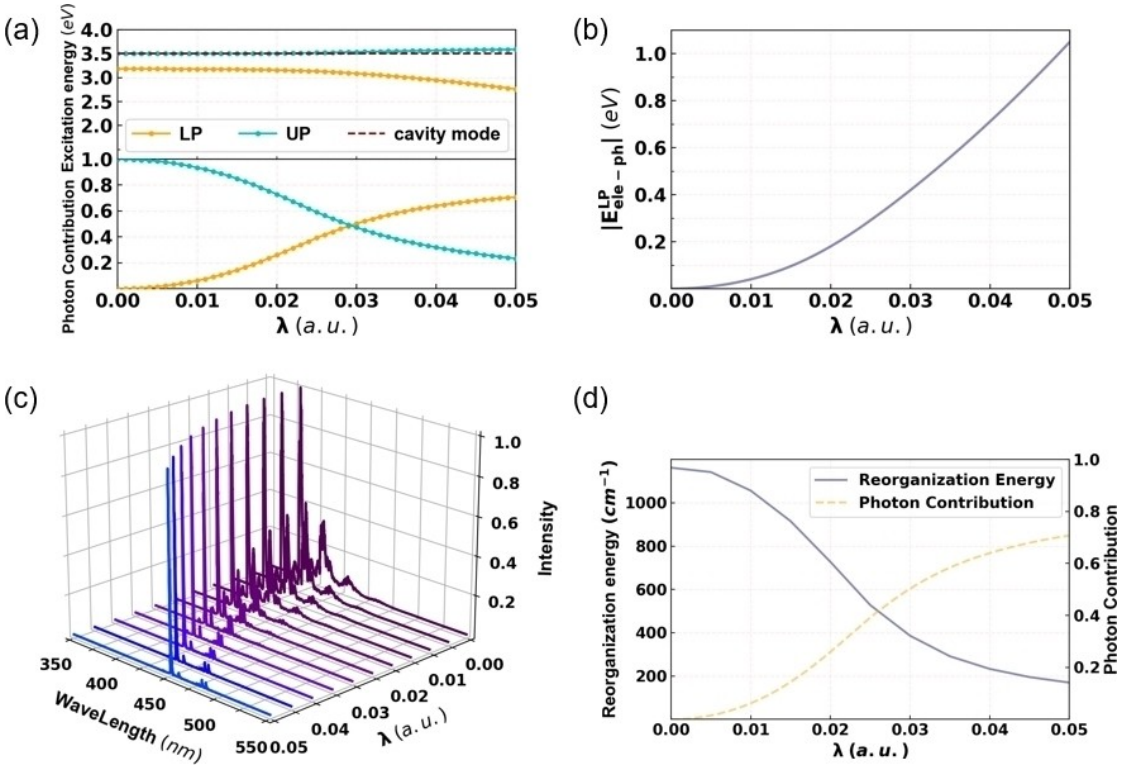

Figure 3. Calculated results for anthracene polariton in **case 1**. (a) The excitation energy and the photon contribution of LP and UP. (b) The light-matter interaction energy of LP with respect to λ. (c) The theoretical emission spectra of LP at various λ values. (d) The photon contribution in LP and the reorganization energy of LP with respect to λ.

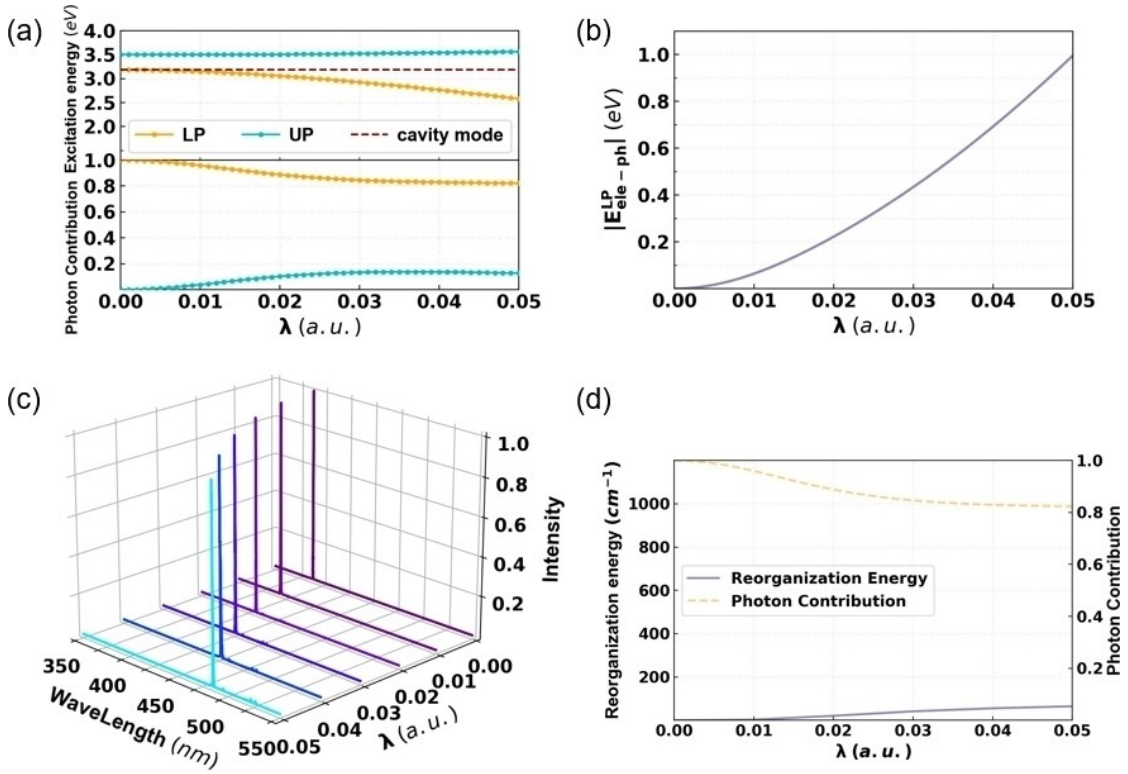

Figure 4. Calculated results for anthracene polariton in **case 2**. (a) The excitation energy and the photon contribution of LP and UP. (b) The light-matter interaction energy of LP with respect to λ. (c) The theoretical emission spectra of LP at various λ values. (d) The photon contribution in LP and the reorganization energy of LP with respect to λ.

becomes dominated by S_1 as λ increases, leading to a decrease in the excitation energy of UP.

We now investigate the composition of the LP and UP, i.e., the photon and exciton contributions to two polariton branches. As λ tends to zero, the LP state becomes the lower energy state between the pure photon state and the pure electronic excited state. Therefore, when $\lambda=0$, for the case of positive detuning (**case 1**), the optimized LP tends towards a pure electronic excited state, whereas when for negative detuning (**case 2**), it tends towards a pure photon state. In the case of positive detuning (**case 1**), the photon contribution in LP gradually increases as λ becomes larger and that in UP decreases [Figure 3(a)]. The contributions of photons in the two states intersect around $\lambda=0.03$, and their combined total is always close to 100%. This process indicates that with increasing the coupling strength, the LP gradually transit from an exciton-dominant state to a photon-dominant state. Moreover, when positive detuning is smaller (when $\hbar\omega_C=3.401$ eV, corresponding to 0.1250 a.u.), the crossover point appears at smaller λ value (0.02 a.u.), as shown in Figure S3(c). Furthermore, as λ increases after the positive detuning crossover point, the photon contribution continue to increase. In the case of negative detuning (**case 2**), the photon contribution in LP shows a decreasing trend starting from 100% with increasing λ [Figure 4(a)]. Additionally, the decrease becomes more substantial with smaller detuning, as shown in Figures S3(a) and S3(b). Regardless of whether it is positive or negative detuning, when λ is large, the photon contribution in LP tends to reach a constant value. We believe that this value is mainly determined by the molecular excited state energy and transition dipole, thus primarily depending on the molecular species. For anthracene, this value is approximately 80%. Additional exciton contributions from higher excited states to the LP state is shown in Figure S10(a) and S10(b). It can be observed that the dominant excitonic contribution in the LP state is S_1, although the contribution of higher excited states increases with the coupling strength, it remains below 1%. This outcome can be attributed to the significant difference between the excitation energy of the higher excited states and the cavity mode photon energy, as well as the relatively small transition dipole moment in the λ direction.

The calculated emission spectra are consistent with the energy and photon contribution calculations. As shown in Figures 3(c) and 4(c), at $\lambda=0$, the emission spectra correspond to the molecular spectra and cavity spectra, respectively, since the LP states in **case 1** and **case 2** are optimized to the S_1 state and the photon state, respectively. In a single-mode cavity without dissipation, the cavity spectrum appears as a sharp line. With the increase of λ, the emission spectra of the LP state exhibit an apparent redshift, and the spectrum in **case 2** shows a greater redshift compared to that in **case 1**. In **case 1**, as λ increases, the vibrational peaks other than the 0–0 peak are gradually suppressed. The emission and absorption spectra of the LP state in **case 1** and **case 2** are separately displayed in Figure S8 for $\lambda=0.02$ and $\lambda=0.03$, corresponding to light-matter interaction energies of approximately 200 meV and

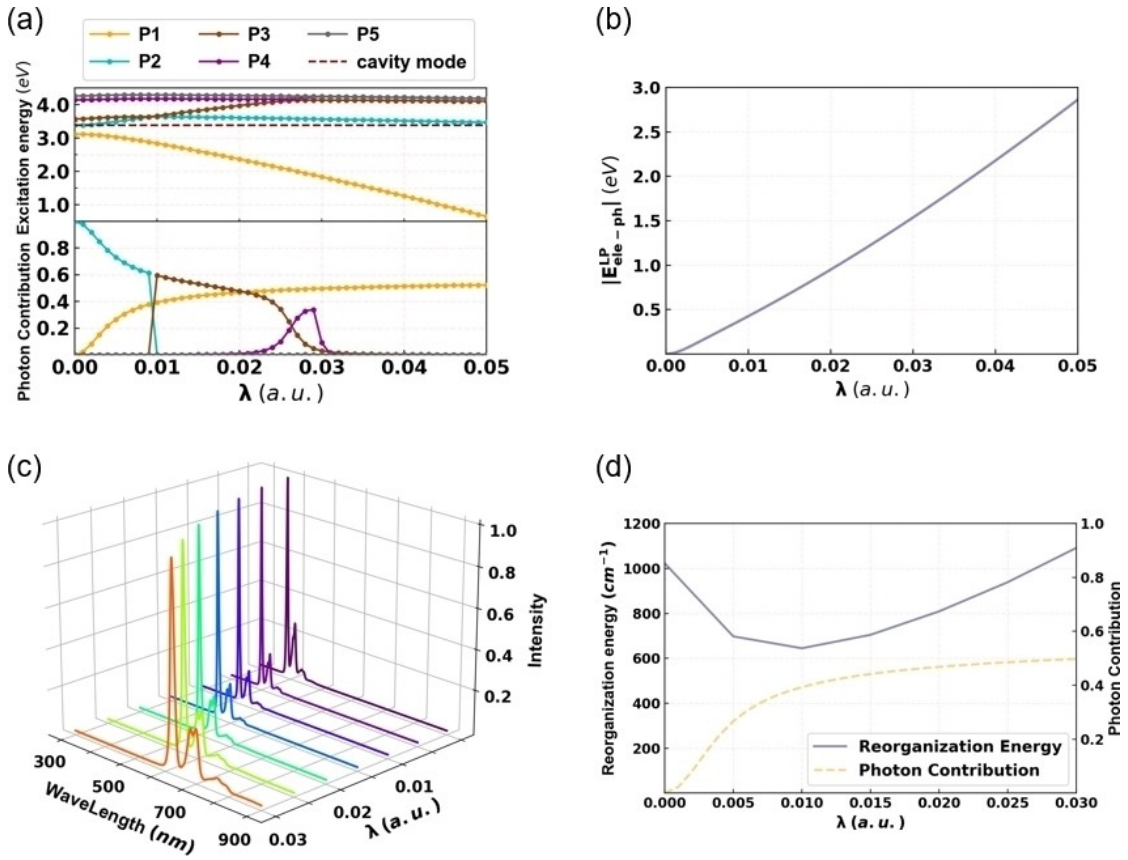

Figure 5. Calculated results for DSB polariton in **case 3**. (a) The excitation energy and the photon contribution of LP and UP. (b) The light-matter interaction energy of LP with respect to λ. (c) The theoretical emission spectra of LP at various λ values. (d) The photon contribution in LP and the reorganization energy of LP with respect to λ.

450 meV, respectively. The LP→S_0 reorganization energy is calculated as shown in Figures 3(d) and 4(d). For **case 1**, the reorganization energy rapidly decreases with the increase of λ, and the corresponding photon contribution of the LP state experiences a rapid increase. Both the decreased reorganization energy and the increased photon contribution of LP indicate the weakened electron-vibration coupling when the coupling strength becomes stronger. This suggests that polaron decoupling might indeed occur in **case 1**. Furthermore, if the region with lower reorganization energy, specifically at $\lambda > 0.03$, is considered the decoupling region, the decoupling condition could be approximated as the light-matter interaction energy (3385 cm^{-1}) being greater than three times the reorganization energy (1316 cm^{-1}). Based on the variation of the photon contribution in the LP state with respect to the detuning, polaron decoupling would occur at higher λ under larger positive detuning conditions. In **case 2**, as λ increases, the exciton contribution gradually mixes into the LP state, and the reorganization energy also increases and approaches that of **case 1**. However, within the tested range of λ, the reorganization energy of LP in **case 2** never exceeds that in **case 1**, which is consistent with the trend of the photon contribution. Correspondingly, as shown in Figures S8(c) and S8(d), up to $\lambda = 0.03$, the LP emission spectrum is still predominantly dominated by the 0–0 peak and remains nearly a sharp line. This spectral shape is reminiscent of the emission spectra of a Bose-Einstein condensate (BEC) laser,[25] which occurs when the LP state is heavily populated. Furthermore, due to the significant overlap between the absorption and emission spectra, we consider the resonant excitation to be highly effective for the LP state. These results indicate that, in the case of negative detuning, the electron-vibration coupling is lower compared to the positive detuning case. Therefore, under both positive and negative detuning conditions, once polaritons can form smoothly, it is expected that polaron decoupling in the LP state will occur in anthracene molecules under sufficiently strong light-matter coupling conditions.

The computed results for the other two molecules, DSB and rubrene, are shown in Figures 5 and 6. The cavity mode energies are set to be the S_1 absorption energies, and both cases correspond to positive detuning. We refer to these cases as **case 3** and **case 4**. Due to the large transition dipole moment of S_1 in DSB (5.453 a.u.), it is more easily coupled to the cavity mode. In **case 3**, the LP state (denoted as P1 in Figure 5(a)) reaches a light-matter interaction energy of approximately 500 meV at $\lambda = 0.01$(as shown in Figure 5(b)), which is significantly larger than the anthracene at the same λ value. The energy of LP also decreases much faster as λ increases compared to the case of anthracene, and the photon contribution stabilizes and converges around 50%. The behavior of

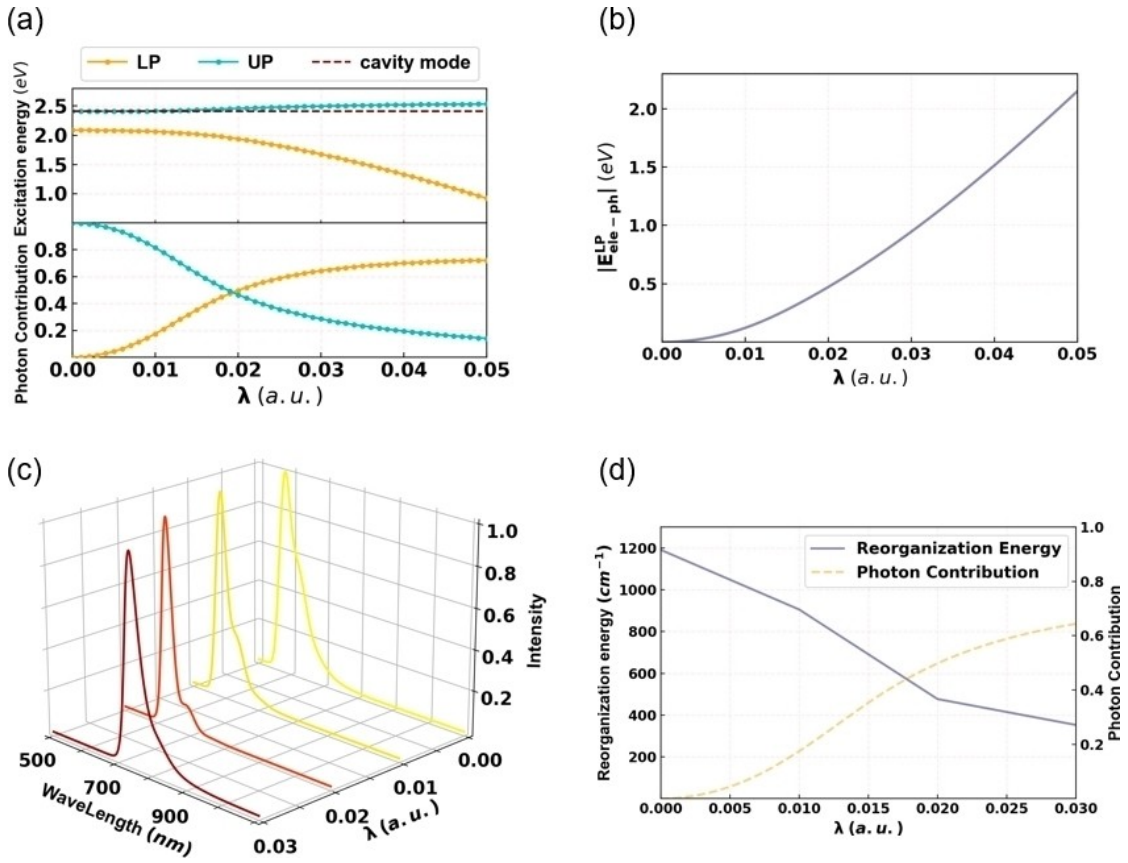

Figure 6. Calculated results for rubrene polariton in **case 4**. (a) The excitation energy and the photon contribution of LP and UP. (b) The light-matter interaction energy of LP with respect to λ. (c) The theoretical emission spectra of LP at various λ values. (d) The photon contribution in LP and the reorganization energy of LP with respect to λ.

higher energy polaritons is more unique, as λ increases, their energy increases sequentially, and the photonic contribution gradually shifts among these states. As for Rubrene (**case 4**), its behavior is closer to that of anthracene. When λ is large, the photon contribution in the LP state converges around 80%, similar to anthracene.

As λ increases, both **case 3** and **case 4** exhibit an increase in the relative intensity of the 0–0 peak and a decrease in LP→S_0 reorganization energy, as shown in Figures 5(c), 5(d) and 6(c), 6(d). Compared to S_1, the LP geometry of rubrene is also significantly closer to S0, as shown in Figure S2. However, in **case 3**, when λ exceeds 0.01, the reorganization energy shows a significant increase, resulting in an increase in the relative intensity of the 0–1 peak in the spectrum. Considering that there is no significant change in the LP component within this range, as shown in Figure S10, this result indicates that the strong-coupling regime might no longer be held. At this point, we consider that the system may enter the regime of ultra-strong coupling,[67] where the light–matter coupling strength is comparable to the transition frequencies in the system. More exploration under such case will be carried out in further studies.

4. Conclusions

Based on QED-TDDFT electronic structure calculations, the spectra of molecular polariton with rich vibronic structure have been predicted using TVCF theory for three molecules, i.e., anthracene, DSB, and rubrene. The calculations have shown that the LP optical emission spectra in the cavity generally exhibit an enhanced intensity for the 0–0 transition along with a reduced reorganization energy compared to the molecular S_1 state, indicating a weakened electron-vibration coupling, which is consistent with Spano's predictions based on model Hamiltonian.[31,32,36,37] Furthermore, the vibrational properties of LP are strongly correlated with the photon contribution. This implies that the design of the cavity can significantly alter the vibrational characteristics of LP over a wide range.

Moreover, due to the presence of the photon component in LP, the weakening of electron-vibration coupling in LP compared to the pure S_1 state may generally occur within a certain range of coupling strengths, although the extent of this effect may vary for different molecular species and photon energies. Although the calculations in this study are limited to single molecules, achieving single-molecule strong coupling is challenging in experiments. In practice, strong light-matter coupling is typically realized through the collective coupling of a large number of molecules. If the light-matter interaction

energy in the calculations corresponds to collective coupling of N molecules, assuming that all molecules interact with the cavity mode identically, the LP excitation energy gradient for a single molecule would become 1/N of the original.[45] Additionally, when the coupling strength is sufficiently large, static disorder contributes minimally to broadening.[68] Therefore, we can anticipate that under collective strong coupling, the LP vibrational properties will closely resemble those of S_0, and polariton decoupling is almost certain to occur, resulting in a much sharper LP spectrum. Hence, approximating the LP using S_0 vibrational properties is quite reasonable.[15] In addition to emission, photophysical processes such as nonradiative internal conversion, intersystem crossing, and charge transfer reactions may also be influenced by the excited-state vibrational structure, which are worth further investigations.

Acknowledgements

This work is supported by the National Natural Science Foundation of China (NSFC) (Grant No. T2350009), Guangdong Provincial Natural Science Foundation, and Shenzhen Science and Technology Program. The work is also supported by the National Science Foundation (Grant No. OAC-2311442).

Conflict of Interests

The authors declare no conflict of interest.

Data Availability Statement

The data that support the findings of this study are available in the supplementary material of this article.

Keywords: Polariton · QED-TDDFT · TVCF · Spectrum · Polaron decoupling

[1] J. Feist, J. Galego, F. J. Garcia-Vidal, *ACS Photonics* **2018**, *5*, 205–216.
[2] D. S. Dovzhenko, S. V. Ryabchuk, Y. P. Rakovich, I. R. Nabiev, *Nanoscale* **2018**, *10*, 3589–3605.
[3] M. Hertzog, M. Wang, J. Mony, K. Börjesson, *Chem. Soc. Rev.* **2019**, *48*, 937–961.
[4] J. Keeling, S. Kéna-Cohen, *Annu. Rev. Phys. Chem.* **2020**, *71*, 435–459.
[5] L. Feng, X. Qi-Hua, *Physics* **2022**, *51*, 445–453.
[6] Z. Jiang, A. Ren, Y. Yan, J. Yao, Y. S. Zhao, *Adv. Mater.* **2022**, *34*, 2106095.
[7] J. A. Hutchison, T. Schwartz, C. Genet, E. Devaux, T. W. Ebbesen, *Angew. Chem. Int. Ed.* **2012**, *51*, 1592–1596.
[8] J. Galego, F. J. Garcia-Vidal, J. Feist, *Phys. Rev. Lett.* **2017**, *119*.
[9] B. Munkhbat, M. Wersäll, D. G. Baranov, T. J. Antosiewicz, T. Shegai, *Sci. Adv.* **2018**, *4*, eaas9552.
[10] N. Thanh Phuc, *J. Chem. Phys.* **2021**, *155*.
[11] J.-H. Song, Y. He, A. V. Nurmikko, J. Tischler, V. Bulovic, *Phys. Rev.* B **2004**, *69*.
[12] T. N. Singh-Rachford, F. N. Castellano, *Coord. Chem. Rev.* **2010**, *254*, 2560–2573.
[13] J. Xu, X. Tang, X. Zhao, H. Zhu, F. Qu, Z. Xiong, *Phys. Rev. Appl.* **2020**, *14*.
[14] D. Polak, R. Jayaprakash, T. P. Lyons, L. Á. Martínez-Martínez, A. Leventis, K. J. Fallon, H. Coulthard, D. G. Bossanyi, K. Georgiou, I. A. J. Petty, J. Anthony, H. Bronstein, J. Yuen-Zhou, A. I. Tartakovskii, J. Clark, A. J. Musser, *Chem. Sci.* **2020**, *11*, 343–354.
[15] Q. Ou, Y. Shao, Z. Shuai, *J. Am. Chem. Soc.* **2021**, *143*, 17786–17792.
[16] B. Zhang, Z. Shuai, *J. Phys. Chem. Lett.* **2022**, *13*, 9279–9286.
[17] J. Sun, H. Hu, D. Zheng, D. Zhang, Q. Deng, S. Zhang, H. Xu, *ACS Nano* **2018**, *12*, 10393–10402.
[18] K. Zhang, Y. Xu, T.-Y. Chen, H. Jing, W.-B. Shi, B. Xiong, R.-W. Peng, M. Wang, *Opt. Lett.* **2016**, *41*, 5740–5743.
[19] A. Mischok, J. Lüttgens, F. Berger, S. Hillebrandt, F. Tenopala-Carmona, S. Kwon, C. Murawski, B. Siegmund, J. Zaumseil, M. C. Gather, *J. Chem. Phys.* **2020**, *153*.
[20] B. Liu, V. M. Menon, M. Y. Sfeir, *APL Photonics* **2021**, *6*, 016103.
[21] A. V. Zasedatelev, A. V. Baranikov, D. Urbonas, F. Scafirimuto, U. Scherf, T. Stöferle, R. F. Mahrt, P. G. Lagoudakis, *Nat. Photonics* **2019**, *13*, 378–383.
[22] J. R. Tischler, M. S. Bradley, V. Bulović, J. H. Song, A. Nurmikko, *Phys. Rev. Lett.* **2005**, *95*.
[23] N. Christogiannis, N. Somaschi, P. Michetti, D. M. Coles, P. G. Savvidis, P. G. Lagoudakis, D. G. Lidzey, *Adv. Opt. Mater.* **2013**, *1*, 503–509.
[24] R. Shinar, J. Shinar, *Journal of Physics: Photonics* **2022**, *4*, 032002.
[25] S. Kéna-Cohen, S. R. Forrest, *Nat. Photonics* **2010**, *4*, 371–375.
[26] M. Slootsky, Y. Zhang, S. R. Forrest, *Phys. Rev. B* **2012**, *86*.
[27] K. S. Daskalakis, S. A. Maier, R. Murray, S. Kéna-Cohen, *Nat. Mater.* **2014**, *13*, 271–278.
[28] T. Ishii, K. Miyata, M. Mamada, F. Bencheikh, F. Mathevet, K. Onda, S. Kéna-Cohen, C. Adachi, *Adv. Opt. Mater.* **2022**, *10*, 2102034.
[29] J. Galego, F. J. Garcia-Vidal, J. Feist, *Phys. Rev. X* **2015**, *5*.
[30] M. Arikan, R. T. Pepino, S. Ingvarsson, I. Shelykh, *Superlattices Microstruct.* **2010**, *47*, 139–144.
[31] F. C. Spano, *J. Chem. Phys.* **2015**, *142*.
[32] F. Herrera, F. C. Spano, *Phys. Rev. A* **2017**, *95*.
[33] I. S. Ulusoy, J. A. Gomez, O. Vendrell, *J. Phys. Chem. A* **2019**, *123*, 8832–8844.
[34] I. S. Ulusoy, O. Vendrell, *J. Chem. Phys.* **2020**, *153*, 044108.
[35] M. A. Zeb, P. G. Kirton, J. Keeling, *ACS Photonics* **2018**, *5*, 249–257.
[36] F. Herrera, F. C. Spano, *Phys. Rev. Lett.* **2016**, *116*, 238301.
[37] F. C. Spano, *J. Chem. Phys.* **2020**, *152*.
[38] M. Ruggenthaler, F. Mackenroth, D. Bauer, *Phys. Rev. A* **2011**, *84*, 042107.
[39] I. V. Tokatly, *Phys. Rev. Lett.* **2013**, *110*.
[40] C. Pellegrini, J. Flick, I. V. Tokatly, H. Appel, A. Rubio, *Phys. Rev. Lett.* **2015**, *115*.
[41] C. Schäfer, M. Ruggenthaler, A. Rubio, *Phys. Rev. A* **2018**, *98*.
[42] J. Flick, D. M. Welakuh, M. Ruggenthaler, H. Appel, A. Rubio, *ACS Photonics* **2019**, *6*, 2757–2778.
[43] R. Jestädt, M. Ruggenthaler, M. J. T. Oliveira, A. Rubio, H. Appel, *Adv. Phys.* **2019**, *68*, 225–333.
[44] J. Yang, Q. Ou, Z. Pei, H. Wang, B. Weng, Z. Shuai, K. Mullen, Y. Shao, *J. Chem. Phys.* **2021**, *155*.
[45] J. Yang, Z. Pei, E. C. Leon, C. Wickizer, B. Weng, Y. Mao, Q. Ou, Y. Shao, *J. Chem. Phys.* **2022**, *156*.
[46] T. S. Haugland, E. Ronca, E. F. Kjønstad, A. Rubio, H. Koch, *Phys. Rev. X* **2020**, *10*.
[47] A. E. DePrince III, *J. Chem. Phys.* **2021**, *154*.
[48] Q. Peng, Y. Niu, Q. Shi, X. Gao, Z. Shuai, *J. Chem. Theory Comput.* **2013**, *9*, 1132–1143.
[49] Z. Shuai, Q. Peng, *Phys. Rep.* **2014**, *537*, 123–156.
[50] Q. Peng, D. Fan, R. Duan, Y. Yi, Y. Niu, D. Wang, Z. Shuai, *J. Phys. Chem. C* **2017**, *121*, 13448–13456.
[51] Q. Ou, Q. Peng, Z. Shuai, *Nat. Commun.* **2020**, *11*.
[52] R. Ianconescu, E. Pollak, *J. Phys. Chem. A* **2004**, *108*, 7778–7784.
[53] C. W. Gardiner, M. J. Collett, *Phys. Rev. A* **1985**, *31*, 3761–3774.
[54] C. Eckart, *Phys. Rev.* **1935**, *47*, 552–558.
[55] Q. Sun, *J. Comput. Chem.* **2015**, *36*, 1664–1671.
[56] Q. Sun, T. C. Berkelbach, N. S. Blunt, G. H. Booth, S. Guo, Z. Li, J. Liu, J. D. McClain, E. R. Sayfutyarova, S. Sharma, S. Wouters, G. K. L. Chan, *WIREs Comput. Mol. Sci.* **2018**, *8*, e1340.
[57] Q. Sun, X. Zhang, S. Banerjee, P. Bao, M. Barbry, N. S. Blunt, N. A. Bogdanov, G. H. Booth, J. Chen, Z.-H. Cui, J. J. Eriksen, Y. Gao, S. Guo, J. Hermann, M. R. Hermes, K. Koh, P. Koval, S. Lehtola, Z. Li, J. Liu, N. Mardirossian, J. D. McClain, M. Motta, B. Mussard, H. Q. Pham, A. Pulkin, W. Purwanto, P. J. Robinson, E. Ronca, E. R. Sayfutyarova, M. Scheurer, H. F. Schurkus, J. E. T. Smith, C. Sun, S.-N. Sun, S. Upadhyay, L. K. Wagner, X. Wang, A. White, J. D. Whitfield, M. J. Williamson, S. Wouters, J. Yang, J. M. Yu, T. Zhu, T. C. Berkelbach, S. Sharma, A. Y. Sokolov, G. K.-L. Chan, *J. Chem. Phys.* **2020**, *153*, 024109.

[58] Z. Shuai, Q. Peng, *Natl. Sci. Rev.* **2016**, *4*, 224–239.
[59] Z. Shuai, *Chin. J. Chem.* **2020**, *38*, 1223–1232.
[60] M. J. Frisch, G. W. Trucks, H. B. Schlegel, G. E. Scuseria, M. A. Robb, J. R. Cheeseman, G. Scalmani, V. Barone, G. A. Petersson, H. Nakatsuji, X. Li, M. Caricato, A. V. Marenich, J. Bloino, B. G. Janesko, R. Gomperts, B. Mennucci, H. P. Hratchian, J. V. Ortiz, A. F. Izmaylov, J. L. Sonnenberg Williams, F. Ding, F. Lipparini, F. Egidi, J. Goings, B. Peng, A. Petrone, T. Henderson, D. Ranasinghe, V. G. Zakrzewski, J. Gao, N. Rega, G. Zheng, W. Liang, M. Hada, M. Ehara, K. Toyota, R. Fukuda, J. Hasegawa, M. Ishida, T. Nakajima, Y. Honda, O. Kitao, H. Nakai, T. Vreven, K. Throssell, J. A. Montgomery Jr, J. E. Peralta, F. Ogliaro, M. J. Bearpark, J. J. Heyd, E. N. Brothers, K. N. Kudin, V. N. Staroverov, T. A. Keith, R. Kobayashi, J. Normand, K. Raghavachari, A. P. Rendell, J. C. Burant, S. S. Iyengar, J. Tomasi, M. Cossi, J. M. Millam, M. Klene, C. Adamo, R. Cammi, J. W. Ochterski, R. L. Martin, K. Morokuma, O. Farkas, J. B. Foresman, D. J. Fox *Gaussian 16 Rev. C.01*, Vol. Wallingford, CT, **2016**.
[61] C. M. Byron, T. C. Werner, *J. Chem. Educ.* **1991**, *68*, 433.
[62] J. Gierschner, M. Ehni, H.-J. Egelhaaf, B. Milián Medina, D. Beljonne, H. Benmansour, G. C. Bazan, *J. Chem. Phys.* **2005**, *123*.
[63] P. Irkhin, A. Ryasnyanskiy, M. Koehler, I. Biaggio, *Phys. Rev. B* **2012**, *86*, 085143.
[64] R. Borrelli, A. Peluso, *J. Chem. Phys.* **2006**, *125*.
[65] A. Peluso, R. Borrelli, A. Capobianco, *J. Phys. Chem. A* **2009**, *113*, 14831–14837.
[66] J. Cerezo, F. Santoro, *J. Chem. Theory Comput.* **2016**, *12*, 4970–4985.
[67] A. Frisk Kockum, A. Miranowicz, S. De Liberato, S. Savasta, F. Nori, *Nature Reviews Physics* **2019**, *1*, 19–40.
[68] C. Climent, J. E. Subotnik, A. Nitzan, *Phys. Rev. A* **2024**, *109*, 052809.

Manuscript received: March 31, 2024
Revised manuscript received: June 10, 2024
Accepted manuscript online: July 10, 2024
Version of record online: September 8, 2024